Heat and Mass Transfer 37 (2001) 315–320 © Springer-Verlag 2001

Heat transfer distribution in rectangular ducts with V-shaped ribs

X. Gao, B. Sundén

Abstract Heat transfer distributions are presented for a rectangular duct with two opposite wide walls arranged with V-shaped ribs pointing upstream or downstream relative to the main flow direction. The rectangular duct has an aspect ratio of 1/8. The parallel V-shaped circular ribs are arranged staggered on the two wide walls. The rib height-to-hydraulic diameter ratio is 0.06, with an attack angle of 60°. The pitch-to-height ratio equals 10. The tested Reynolds numbers range from 1000 to 6000. The test surface is sprayed with black paint and then liquid crystal, and a steady state method is adopted to obtain the temperature distribution between adjacent ribs. The secondary flow caused by the angled ribs creates different spanwise variation of the heat transfer coefficient on the rib-roughened wall for different V-rib orientations. Interaction between heat transfer and secondary flow is analyzed. In the streamwise direction, the temperature distribution shows a sawtooth behavior between a pair of adjacent ribs. Local Nusselt numbers are presented between a pair of adjacent ribs, and based on these the average Nusselt numbers are calculated to investigate the augmentation of heat transfer by the presence of the V-shaped ribs.

1 Introduction

Periodic ribs are frequently employed in heat exchangers to enhance the heat transfer process. The heat transfer distribution and enhancement caused by parallel ribs has been investigated [1]. V-shaped ribs originated from the concept that angled ribs can act as longitudinal vortex generator and provide heat transfer augmentation. It is then assumed that V-shaped ribs can principally double the high heat transfer region and provide even higher heat transfer coefficients (see, e.g., [2]). Because the flow field is disturbed by the presence of the ribs and the orientation of the V-shaped ribs will induce different types of secondary flow, and the local heat transfer distributions are also different.

Han et al. used thermocouples to investigate the heat transfer of a square duct with 45 and 60° V-shaped ribs, and the ribs could point in the main flow direction or in the opposite direction [3]. The ribbed walls were in-line and the Reynolds number covered the range of 15 000–90 000. The V-shaped ribs directed opposite to the main flow provided the highest heat transfer enhancement. Taslim et al. employed liquid crystal thermography to study the heat transfer enhancement caused by V-shaped ribs on two opposite walls of a square duct [2]. The 45° angled ribs were arranged with a fixed pitch-to-height ratio of 10. In the whole Reynolds number range of 5000–30 000, for the blockage ratio (e/D_h) of 0.083, it was revealed that V-shaped ribs pointing downstream produced the highest heat transfer enhancement. These results contradict those of [3]. In another investigation, Ekkad and Han measured the heat transfer of a two-pass square duct with 60° V-ribs using liquid crystal thermography. The Reynolds numbers were from 6000 to 60 000 [4]. The Nusselt number ratio distributions for the first pass with V-ribs pointing in the opposite direction to the main flow showed the same behavior as those from [2]. For the second pass where the ribs pointed in the same direction as the main flow, the local Nusselt numbers were more affected by the combined effect of the ribs and the sharp 180° turn. Therefore, to reveal the effect of the orientation of V-ribs on the local and average heat transfer coefficient distributions further investigations are required, especially for the low Reynolds numbers range and for aspect ratio different from unity.

The present study concentrates on the local heat transfer distribution between adjacent pairs of V-ribs in the fully developed periodic flow region in the Reynolds number range of 1000–6000 for a rectangular duct. The parallel V-ribs were arranged staggered on the two opposite wide walls and aligned with or against the main flow direction. The interaction between heat transfer and secondary flow pattern is discussed based on the different heat transfer distributions caused by the orientations of the V-ribs. Both the local and average Nusselt numbers are presented.

2 Experimental apparatus and procedure

2.1 Experimental setup

The experimental setup is shown schematically in Fig. 1. The liquid crystal technique was employed to measure the heat transfer coefficients between consecutive ribs in the test section, because it has the ability to "map" the thermal field so as to provide details of the temperature distribution. Before the execution of the visualization experiment,

Received on 15 May 2000

X. Gao, B. Sundén (✉)
Lund, Sweden

Financial support from Valeo Engine Cooling Systems and AB Volvo is kindly acknowledged.

the liquid crystal was calibrated to get the monotonic relationship between the temperature of the liquid crystal and the measured hue of the reflected light to the surface. The uniform temperature calibration was adopted. The hue value range of 60 ~ 90 was used in the calculation because it showed best performance in the calibration curve. This hue value range corresponded to the green color in the liquid crystal image and the details were introduced in [5].

The experimental study was carried out for a rectangular duct with V-shaped ribs on two wide walls. The sidewalls of the entire test duct were made of plexiglas plates to provide optical access for the liquid crystal measurements. In order to thermally insulate the test section, insulation materials were used to cover the outer surfaces of the test section except a small part left for the CCD camera to catch images.

The test section consists of a 700 mm long smooth section followed by a rib-roughened section of equal length. The duct thickness is 10 mm with a cross section of 14.5 × 112.5 mm. In order to observe the periodic results of the present prediction, the measurements were carried out for the region of $50 < x/D_h < 52$ from the inlet of the rectangular channel, where both the hydrodynamic and the thermal fully developed periodic conditions are considered to have been reached. In practice, the onset of the periodic fully developed region occurs about 5 hydraulic diameters downstream of the ribbed duct inlet for turbulent flow, as reported by Chang et al. [6].

Two pieces of a thermal foil made of Inco 600 with a thickness of 0.1 mm, were adhered at the two opposite wide inner surfaces of the rib-roughened section. The heater on the wall, where the liquid crystal was sprayed, covered the entire 700 mm ribbed section length, but the heater on the opposite wall, through which images were taken, covered only 550 mm length, so that the remainder could provide optical access for the CCD camera. AC-stabilized power supply to the foil had been provided through a variable transformer so that the uniform heat flux to the walls could be varied as desired. On the surface of the heater, black paint and then the liquid crystal were sprayed for the area corresponding to $50 < x/D_h < 52$.

The ribs, which were made of plastic tubes, had a circular cross section with a diameter of 1.5 mm. The ribs were glued on the two broad walls using double-sided adhesive tape in a staggered arrangement. This rib configuration is shown in Fig. 2. The rib height-to-hydraulic diameter ratio, e/D_h was 0.06. The rib pitch-to-height ratio p/e, was 10. The ribs had an angle of 60° to the main flow direction.

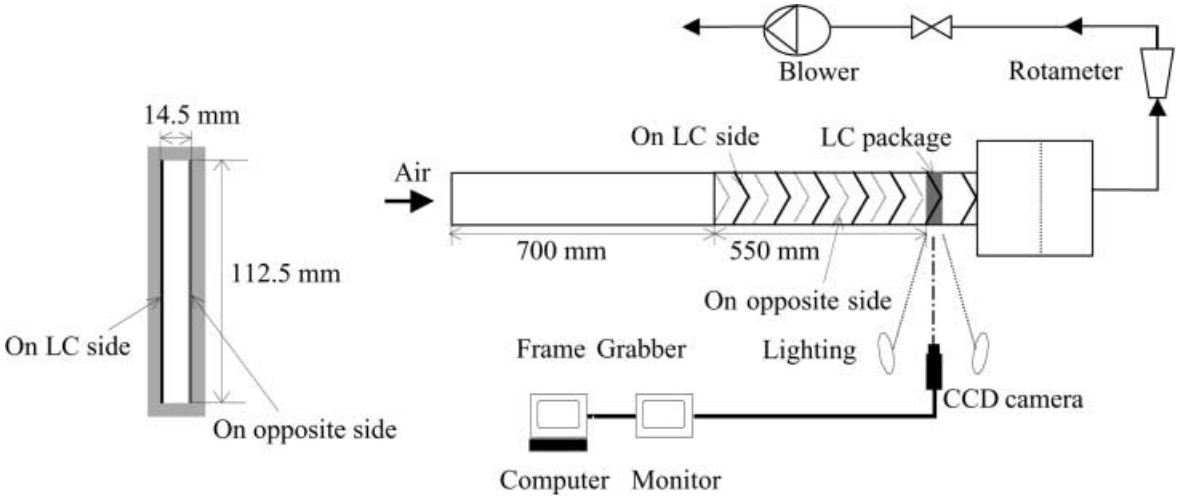

Fig. 1. Schematic drawing of the experimental setup

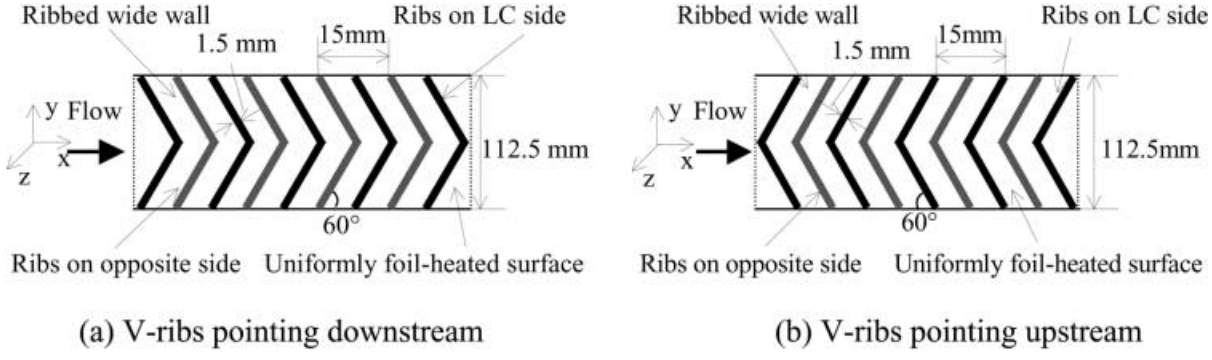

Fig. 2. Rib configurations

2.2
Experimental procedure

The airflow rates were measured by two Krohne rotameters (flow ranges 0.8–8.0 and 3–30 m^3/h, respectively), with an error less than ±3%. The Reynolds number is calculated by $\mathrm{Re} = \frac{u_m D_h}{\nu}$. The entrance and exit air temperatures were measured directly by thermocouples. The local bulk air temperature was evaluated by assuming a linear air temperature rise along the duct. An in-house developed program was used to monitor Reynolds numbers at different temperature conditions and then to adjust the flow valve to keep the Reynolds numbers stable. The supplied heat flux could be calculated from the electrical current and voltage. The corresponding smooth duct area was assumed to be the heat transfer area. The conduction heat loss from the test duct was determined separately at a no flow condition and it was then deducted from the total heat flux to get the heat flux convected away by flowing air.

Before the experimental results of the steady state condition are displayed, it is necessary to clarify the steady state of each run. The steady state was considered to be achieved when the enthalpy rise of air equaled the supplied heat deducted by the conduction loss. For a fixed Reynolds number, the electric power input into the heating foil was adjusted to produce the first reference green color of the liquid crystal on the ribbed surface. A uniform heat flux was supplied to the ribbed surface, after the system reached thermal equilibrium, i.e., the overall heat balance had been reached and the isochromes on the liquid crystal remained stationary, images were taken by a CCD camera. Each image was then transferred through a frame grabber for storage and further image processing. This area covered by the reference color corresponded to locations of lowest heat transfer coefficients. By increasing the power input to the heater, the reference color on the surface moved to the next locations, where higher heat transfer were assumed, and another image was taken. This procedure was repeated until the entire surface had been covered with the reference color in a sequence of time. For each certain Reynolds number, 10 ∼ 30 images were acquired. These images were then converted from RGB matrices to HSI matrices, where *H*, the hue value, was used to represent specific temperature from the calibration curve. The temperature field was then digitized and extracted by using a commercial software package running on a PC.

3
Results and discussion

3.1
Data evaluation

In the present study, the experimental results are presented in terms of local Nusselt numbers, Nu, which can be derived directly from the heat flux and the temperature difference. The air thermal properties are evaluated at the film temperature, which is calculated as the average of the wall temperature and the bulk temperature. One has:

$$\mathrm{Nu} = q_w D_h / ((T_{wall} - T_{bulk}) k_f) \quad (1)$$

Average Nusselt numbers are estimated as weighted mean values of the local Nusselt numbers obtained from Eq. (1)

$$\mathrm{Nu}_{av} = \sum_{i=1}^{N} \mathrm{Nu}_i r_i \Big/ \sum_{i=1}^{N} r_i \quad (2)$$

where r_i is the number of pixels for the hue value considered, and *N* is the number of areas of constant Nusselt number.

The average Nusselt number is compared to the fully developed smooth duct value. For Re < 2000, the constant Nusselt number Nu_0 = 6.49 is adopted according to, e.g., [7]. For Re > 2000, the Nusselt number is compared to the Dittus–Boelter equation for smooth circular ducts, see, e.g., [8]. This correlation reads

$$\mathrm{Nu}_0 = 0.023\,\mathrm{Re}^{0.8}\,\mathrm{Pr}^{0.4} \quad (3)$$

The experimental uncertainty in the Nusselt number, based on the method presented in [9], and described in [5], is estimated to be within ±7.2%.

3.2
V-ribs pointing upstream (<<)

Figure 3 shows the initial RGB images taken for the V-shaped ribs pointing upstream compared to the flow direction at different heat fluxes and at Reynolds number of

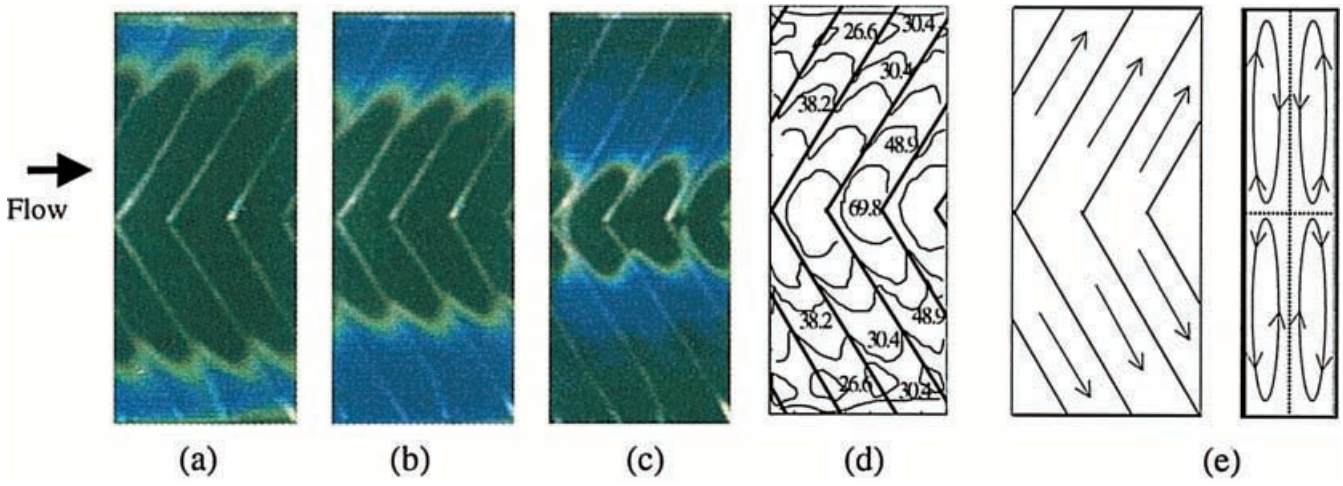

Fig. 3. V-shaped ribs pointing upstream compared to the main flow direction at Reynolds number of 6000. **a** $q_w = 354$ W/m^2, **b** $q_w = 437$ W/m^2, **c** $q_w = 660$ W/m^2, **d** Local Nusselt number contours on the V-rib-roughened surface, **e** Schematic pattern of the secondary flow induced by V-ribs

6000. The green color of the RGB images was assigned as the reference color. As one can see, the reference green color on the surface moves from both the bottom side and the top side to the central area as the heat flux increases as the images in Fig. 3a–c show. Because the temperature difference used in the calculation of the Nusselt number did not vary so much, the magnitude of the local heat transfer coefficient is followed by the heat flux increase. This means that the heat transfer coefficient on the rib-roughened wall has a significant spanwise variation, with low levels at both the bottom and the top ends of the duct, and high levels at the central area where the V-shaped ribs meet. For all the Reynolds number tested, the images have essentially a very similar fashion as the ones shown at a Reynolds number of 6000.

Some representative contours of constant Nusselt number are shown in Fig. 3d. It can be seen that at the top and bottom edges, the local Nusselt number is low. The magnitude is close to that of the smooth duct wall. In the central apex area, the local Nusselt number is much higher, about 3 times that of the smooth duct wall.

The significant spanwise variation of the heat transfer coefficient is attributed to the angled V-ribs. The V-ribs generate two double-cell counter-rotating vortices that extend over the whole cross section. The temperature boundary layer is thin and the local heat transfer is high in the downwash regions and low in the upwash regions, as shown in Fig. 3e. The longitudinal vortex of the fluid guaranties that the heat taken up by a fluid particle at the wall is transported away from the wall and downstream. By the time it returns close to the wall, it has been cooled by the bulk temperature and then can again take up heat from the wall [10]. The vortex motion results in occurrence of the lowest Nusselt numbers at the bottom and top edges in the upwash regions, but it reaches values about three times in the strong downwash areas at the apex region. The average Nusselt number is enhanced as will be shown later.

3.3
V-ribs pointing downstream (>>)

Figure 4 shows the initial RGB images taken for the V-shaped ribs pointing downstream at different heat fluxes and at a Reynolds number of 6000. The reference green color on the surface occurred in the central area of the V-ribs at the lowest heat flux, and then moved from the central area to both the bottom and the top sides symmetrically with an increase of the heat flux, as the images (a), (b) and (c) show. The spanwise heat transfer coefficient distribution is totally different from that of V-ribs pointing upstream, see Fig. 3. For the central part where the V-ribs pointing upstream induced the highest heat transfer coefficient, the V-ribs pointing downstream produce the lowest heat transfer coefficient. For both the bottom and top sides, where the V-ribs pointing upstream induced the lowest heat transfer coefficient, the V-ribs pointing downstream produce the highest heat transfer coefficient. Again, for each half part of the V-ribbed wall, the heat transfer coefficient is lowest at one end of the rib, and highest at the other end. For the other Reynolds numbers tested, the images are essentially very similar.

For the V-ribs pointing downstream relative to the main flow direction, the ribs also create two double-cell counter-rotating vortices but in an opposite direction compared to the ribs pointing upstream. The moving vortices carry warmer air towards the central area from the top and bottom edges, as illustrated in Fig. 4e. Therefore, the lowest Nusselt number occurs in the center duct area and increases all the way to the junctions between the ribbed wall and the top and bottom smooth walls. The overall heat transfer is also enhanced, see a later section.

3.4
Streamwise distribution

In the flow direction, the green color distribution has common characteristics for both V-ribs directions. It shows a sawtooth distribution between a pair of adjacent ribs, as evident in Figs. 3 and 4. This means that the temperature varies along the x-axis. If Fig. 3 is treated as an example, one can observe the reference color, starting from downstream of a rib, going back to locations nearer to top and bottom ends in the region between ribs, and then moves forward to the apex region upstream of the

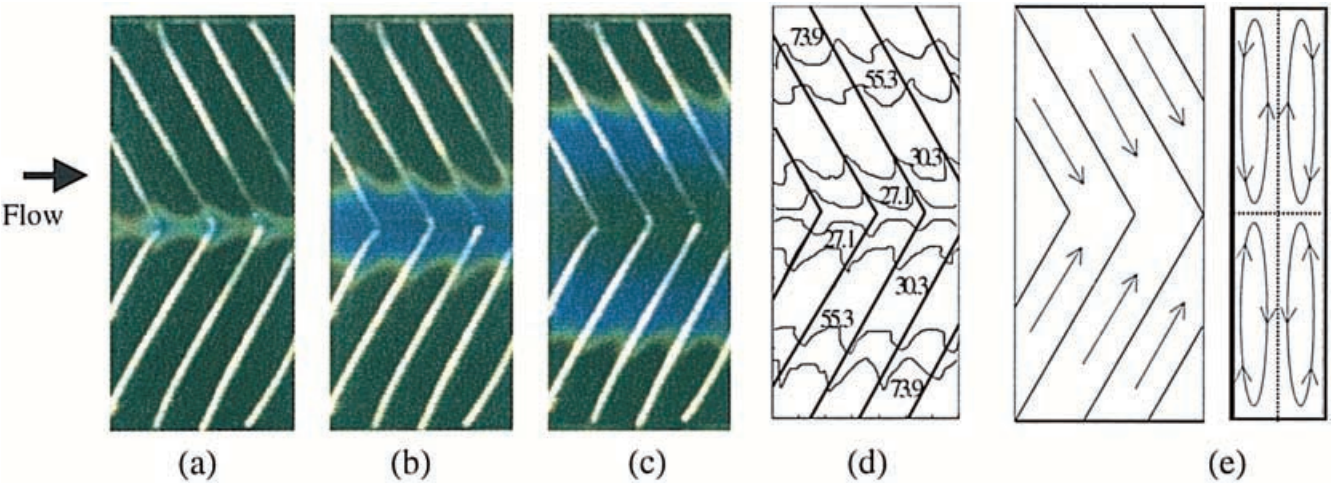

Fig. 4. V-shaped ribs pointing downstream of the main flow direction at Reynolds number of 6000. **a** $q_w = 383$ W/m^2, **b** $q_w = 455$ W/m^2, **c** $q_w = 575$ W/m^2, **d** Local Nusselt number contours on the V-rib-roughened surface, **e** Schematic pattern of the secondary flow induced by V-ribs

next rib. The different temperatures mean that the heat transfer coefficients are different. The Nusselt numbers in the region of the rib's rear edge are the smallest ones due to nearly stagnant flow. The Nusselt number reaches the highest value at locations between a pair of adjacent ribs, and then decreases again close to the next rib. For all the Reynolds numbers tested, the downstream distance from each rib where the highest heat transfer coefficients occur is not the same, but becomes shorter as the Reynolds number increases.

The streamwise distribution of the heat transfer coefficient can be explained by the flow reattachment and redevelopment. In fully turbulent flow, depending on the downstream distance to the next rib, the recirculating flow cells developing downstream may reattach at the duct wall, and the flow then commences to develop again. Due to redevelopment of a boundary layer and the possible enhancement of turbulence near this reattachment point, the heat transfer is enhanced. As an effect relatively low wall temperatures at the midrib locations occur, see, e.g., [11]. It is shown clearly in Figs. 3 and 4 that the midrib locations have the lowest temperatures at a fixed heat flux. Thus the highest heat transfer coefficients occur here. At the same time, one can observe that there are two temperature peaks immediately downstream and upstream of each rib.

3.5
Wall averaged Nusselt number

The wall averaged Nusselt numbers are estimated as weighted mean values from local Nusselt numbers by Eq. (2) over the surface of $50.2 < x/D_h < 51.8$. Figure 5 shows the average Nusselt number versus Reynolds number. As can be seen the average Nusselt number is enhanced by both orientations of the V-shaped ribs and increases with an increase in Reynolds number. In the tested Reynolds number range, the enhanced average Nusselt numbers caused by the V-ribs pointing downstream are higher than those caused by the V-ribs pointing upstream. This conclusion agrees with [2], in which the authors also used liquid crystal thermography to investigate the local heat transfer distribution. Nevertheless, it is contradictory to the results in [12], which investigated the overall heat transfer performance of smaller scale rib-roughened ducts and concluded that V-ribs pointing upstream provided higher heat transfer coefficient. In that case, both the duct walls and the ribs were made of copper, so that highly conductive ribs were involved in heat transfer process. The ribs were arranged more sparsely with the pitch-to-diameter ratio of 50. Constant wall temperature was adopted as the boundary condition. Another possible reason might be that the heat transfer performance in the fully developed region is different from that for the whole length duct if entrance effects are important. Reference [13] reported that although for some rib arrangements, the heat transfer coefficient decreased to a steady level as the flow developed to the fully developed region, the heat transfer did not decrease in the downstream region but continued to increase throughout the entire length for other periodic rib arrangements.

The difference between the V-ribs with different orientations is probably caused by different secondary flow patterns induced by the V-ribs of different orientations, as analyzed previously. The V-shaped ribs pointing upstream produced high heat transfer in the central duct region but the heat transfer was much weaker at both the top and bottom edges. However, for the case of the V-shaped ribs pointing downstream, although the central apex area had low heat transfer, the edges had the highest heat transfer coefficients. This results in the fact that the overall heat transfer enhancement of V-ribs pointing downstream is higher than that of V-ribs pointing upstream.

It should be noted that because the ribs were not sprayed with liquid crystal, there is no thermal information about these. The overall Nusselt numbers should be higher provided that highly conductive ribs were utilized because the rib surface is always involved in the heat transfer process. However, the present study provides continuous heat transfer distributions between a pair of adjacent ribs caused by the ribs. For the same V-shaped ribs with different orientation, the local heat transfer fields are totally different. This helps to understand the roles of the different secondary flows induced by the V-ribs, and their usefulness for industrial heat transfer process. The liquid crystal technique enabled presentations of the entire local Nusselt number distributions between the V-ribs.

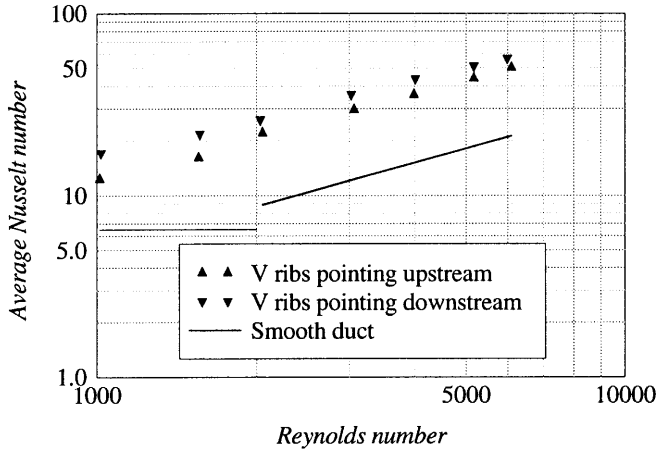

Fig. 5. Average Nusselt number versus Reynolds number

4
Conclusions

The liquid crystal thermography has been used to obtain local Nusselt number distributions. With a real-time image capturing technique, the high spatial resolution with pixel by pixel processing provided an accurate heat transfer tool. The conclusions based on the results are as follows:

(1) Nusselt number distributions are periodic between adjacent ribs.

(2) For all tested Reynolds numbers, the distributions of local Nusselt number are similar, which means that the secondary flow induced by the V-ribs has been established at Reynolds number as low as 1000.

(3) In the direction of the main flow, the local Nusselt number is smallest immediately downstream of each rib, but then increases to the highest value around the mid point between a pair of ribs and finally reaches another low value upstream of the next rib.

(4) The heat transfer coefficient shows a significant spanwise variation. For the V-ribs pointing upstream of the main flow direction, the local Nusselt numbers are lowest on both the top and bottom sides, while the highest values occur in the central duct area. For the V-ribs pointing downstream of the main flow direction, the heat transfer distribution is opposite, the central apex region has the lowest Nusselt number and the junctions between the ribbed wall and the top and bottom smooth walls have the highest values. This spanwise variation is attributed to different secondary flows induced by the orientations of the angled V-ribs.

(5) In Reynolds number range of 1000–6000, in the test area where the flow is considered to have reached the fully developed periodic region, the V-ribs pointing downstream provide higher heat transfer level than V-ribs pointing upstream.

References

1. **Gao X; Sundén B** Heat Transfer Measurements in a Rectangular Duct with Inclined Ribs Using Liquid Crystal Thermography. 34th National Heat Transfer Conference. NHTC2000-12091 (2000) August 20–22, Pittsburgh, USA
2. **Taslim ME; Li T; Kercher DM** (1996) Experimental heat transfer and friction in channels roughened with angled, V-shaped, and discrete ribs on two opposite walls. ASME J Turbomachinery 18: 20–28
3. **Han JC; Zhang YM; Lee CP** (1991) Augmented heat transfer in square channels with parallel crossed, and V-shaped angled ribs. ASME J Heat Transfer 113: 590–596
4. **Ekkad SV; Han JC** (1997) Detailed heat transfer distributions in Two-pass square channels with rib turbulators. Int J Heat Mass Transfer 40: 2525–2537
5. **Gao X; Sundén B** (2000) Detailed measurements of heat transfer coefficients in a rectangular duct using hue-based calibrated liquid crystal. Int Commun Heat Mass Transfer 27: 13–22
6. **Chang SW; Su LM; Hwang CC; Yang TL** (1999) Heat transfer in a reciprocating duct fitted with transverse ribs. Experimental Heat Transfer 12: 95–115
7. **Kakac S; Shah RK; Aung W** (1987) Handbook of Single-Phase Convective Heat Transfer. J. Wiley & Sons Inc., New York
8. **Rohsenow WM; Hartnett JP** (1973) Handbook of Heat Transfer. McGraw-Hill Inc., New York
9. **Moffat RJ** (1988) Describing the uncertainties in experimental results. Experimental Thermal and Fluid Science 1: 3–17
10. **Fiebig M** (1996) Vortices: Tools to Influence Heat Transfer-Recent Developments. In: Celata GP; Marco P Di; Mariani A (Eds) Proceedings of the 2nd European Thermal Sciences Conference, pp. 41–56, Edizioni ETS, Rome
11. **Webb RL** (1994) Principles of Enhanced Heat Transfer. J. Wiley & Sons Inc., New York
12. **Olsson CO; Sundén B** (1998) Experimental study of flow and heat transfer in rib-roughened rectangular channels. Experimental Thermal and Fluid Science 16: 349–365
13. **Metzger DE; Fan CS; Yu Y** (1990) Effects of Rib Angle and Orientation on Local Heat Transfer in Square Channels with Angled Roughness Ribs. In: Shah RK; Kraus AD; Metzger DE (Eds) Compact Heat Exchangers, pp. 151–167, Hemisphere Publishing Corporation
14. **Sundén B** (1999) Enhancement of convective heat transfer in rib-roughened rectangular ducts. Enhanced Heat Transfer 6: 89–103